Identification of wave forces on a floating bridge from acceleration and wave elevation data using inverse methods and wave field reconstruction

Petersen, Øyvind Wiig; Øiseth, Ole; Lourens, Eliz-Mari

Publication date
2018

Document Version
Accepted author manuscript

Published in
Proceedings of the ISMA 2018 International Conference on Noise and Vibration Engineering

Identification of wave forces on a floating bridge from acceleration and wave elevation data using inverse methods and wave field reconstruction

Øyvind Wiig Petersen [1], **Ole Øiseth** [1], **Eliz-Mari Lourens** [2]
[1] NTNU, Norwegian University of Science and Technology, Department of Structural Engineering
7491 Trondheim, Norway
e-mail: **oyvind.w.petersen@ntnu.no**

[2] Delft University of Technology
2628 CN Delft, The Netherlands

Abstract
Knowledge of the ambient loads are important for assessing the dynamic behavior of long-span bridges. However, the assumptions in the adopted load models used in the dynamic analysis leads to uncertainties in e.g. reliability assessments. To reduce the uncertainties, full-scale studies of the loads on existing structures can be performed. Recently developed methods for inverse identification can estimate the unknown forces on a structure using a limited set of dynamic response measurements and a numerical model of the structure. In this contribution, a pilot study of full-scale force identification is performed in a practical case study of the Bergsøysund bridge, a pontoon bridge with a floating span of 840 m. A state of the art filtering technique for input estimation is applied to identify the wave forces on the bridge using measured acceleration data. This article also presents a method for frequency-domain reconstruction of the wave forces, based on a parametric wave field model from measured wave elevation data. The obtained force estimates from the two approaches shows a reasonable agreement. The practical use of the identification techniques are reviewed from the viewpoint of this case study and sources of uncertainties are discussed.

1 Introduction

Floating bridges with spans of 3-5 kilometers are currently being reviewed as a fjord-crossing solution in the infrastructural project Coastal Highway Route E39 in Norway. Suspension bridges with floating towers [1] or pontoon-type bridges [2] are two of the considered concepts. A good understanding of the dynamic behavior of such bridges is essential to ensure the structural safety through the life-time. However, the dynamic behavior is uncertain due to the complexity, novelty and operational environment of these structures. The floating bridges must endure large-amplitude vibrations since the natural frequencies occur in the super-low region (< 0.05 Hz) that is prone to wind and second-order wave forces, as well as in the frequency range of swell and wind sea ($\sim [0.05, 0.3]$ Hz).

In the design phase, established load models dictated by design codes are used to evaluate the dynamic response of the structure. One approach to better understand the true loading is to perform full-scale measurements. This can either be performed on the desired structure after it is built, or alternatively, on already existing similar structures to learn about the in-operation behavior. The dynamic loads are however not possible to measure directly in full-scale, which has lead to the development of inverse methods for identification of forces. These methods utilize response measurements together with a system model to estimate the input

forces on a structure.

This article presents a case-study of full-scale force identification on the Bergsøysund bridge, an existing pontoon-type bridge with a floating span of 840 m. The bridge has been monitored since 2013, and the extensive measurement data has been used in for example studies of response statistics [3], operational modal analysis [4], and full-field response estimation [5]. The force identification method used in the presented study is a joint input-state estimation algorithm [6, 7], a popular Kalman-type filtering method. In addition, separate method for frequency-domain reconstruction of the wave forces from wave elevation data is considered.

2 The Bergsøysund bridge

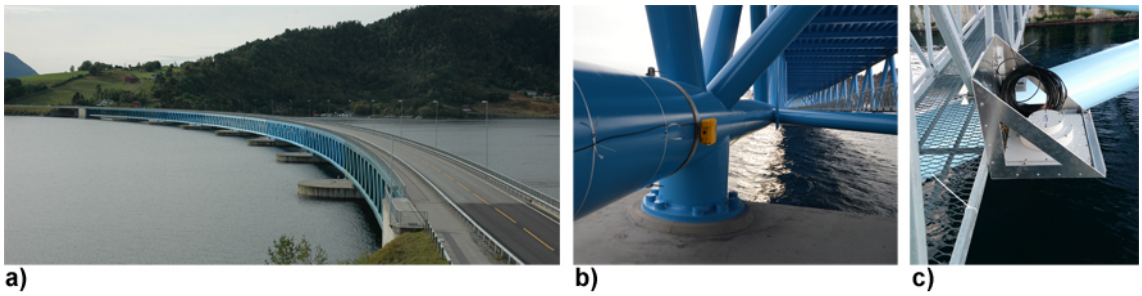

Figure 1: a) The Bergsøysund bridge seen from the northeast end; b) acceleration sensor mounted on the truss; c) wave radar mounted on the walkway.

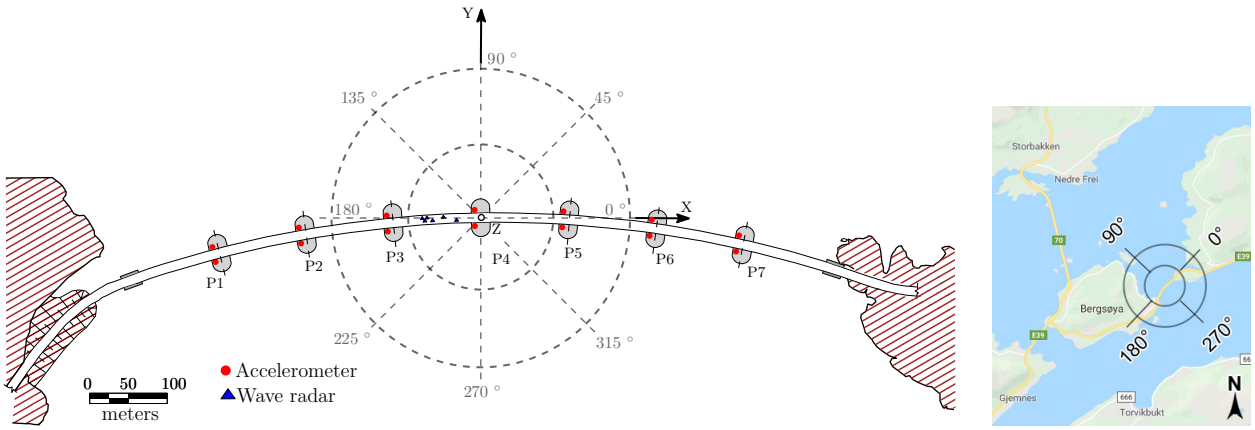

(a) (b)

Figure 2: a) Overhead view of the Bergsøysund bridge showing the locations the accelerometers and wave radars. The compass indicates the definition of the wave direction; b) surrounding area of the bridge (Google maps, 2018).

2.1 Description of the bridge and monitoring system

The Bergsøysund bridge (Fig. 1 a) is located on the northwest coast of Norway. The bridge is 840 m long, and consists of a steel truss that is supported by seven pontoons. The structure is only anchored to the ground at the ends, which makes it very flexible and susceptible to dynamic excitation from wave actions on the pontoons. The bridge is surrounded by other islands and fjords (Fig. 2 b), causing the waves to mainly approach from the north sector ($\sim [30°, 90°]$) or the south sector ($\sim [220°, 320°]$).

A monitoring system at the site records the triaxial acceleration response in 14 locations (Fig. 1 b) and the wave elevation in six locations (Fig. 1 c). The positions of these sensors are shown in Fig. 2 a. More details about the monitoring system are given in [3].

2.2 State-space system model in the time-domain

This section gives a brief overview of how a time-domain state-space model of a floating bridge can be established. The bridge is discretized into n_{DOF} degrees of freedom (DOFs), and is assumed to be excited primarily by n_p wave forces. The governing equations of motion can be formulated in the frequency-domain as follows:

$$-\omega^2\big(\mathbf{M}_s+\mathbf{M}_h(\omega)\big)\mathbf{u}(\omega)+i\omega\big(\mathbf{C}_s+\mathbf{C}_h(\omega)\big)\mathbf{u}(\omega)+\big(\mathbf{K}_s+\mathbf{K}_h\big)\mathbf{u}(\omega)=\mathbf{L}_p\mathbf{p}_w(\omega) \tag{1}$$

The vectors and matrices and their respective sizes are summarized below:

- $\mathbf{u}\in\mathbb{R}^{n_{DOF}}$: response vector
- $\mathbf{p}_w\in\mathbb{R}^{n_p}$: wave force vector
- $\mathbf{L}_p\in\mathbb{R}^{n_{DOF}\times n_p}$: force selection matrix
- $\mathbf{M}_s\in\mathbb{R}^{n_{DOF}\times n_{DOF}}$: structural mass
- $\mathbf{C}_s\in\mathbb{R}^{n_{DOF}\times n_{DOF}}$: structural damping
- $\mathbf{K}_s\in\mathbb{R}^{n_{DOF}\times n_{DOF}}$: structural stiffness
- $\mathbf{M}_h(\omega)\in\mathbb{R}^{n_{DOF}\times n_{DOF}}$: hydrodynamic mass
- $\mathbf{C}_h(\omega)\in\mathbb{R}^{n_{DOF}\times n_{DOF}}$: hydrodynamic damping
- $\mathbf{K}_h\in\mathbb{R}^{n_{DOF}\times n_{DOF}}$: restoring stiffness

The mass, damping and stiffness matrices are obtained from a finite element model of the structure coupled with a fluid-structure interaction model of the pontoons [8].

For purposes of force identification using time-domain filter techniques, it is common to establish a reduced-order modal model [6]. Here, we use the modal base $\mathbf{\Phi}\in\mathbb{R}^{n_{DOF}\times n_m}$ obtained from the following eigenvalue problem:

$$[\mathbf{K}_s+\mathbf{K}_h-\omega_j^2(\mathbf{M}_s+\mathbf{M}_{h,\infty})]\boldsymbol{\phi}_j=\mathbf{0}\quad,\quad(\mathbf{M}_{h,\infty}=\lim_{\omega\to\infty}\mathbf{M}_h(\omega)) \tag{2}$$

$$\mathbf{\Phi}=\begin{bmatrix}\boldsymbol{\phi}_1 & \boldsymbol{\phi}_2 & \dots & \boldsymbol{\phi}_{n_m}\end{bmatrix} \tag{3}$$

However, the traditional mode-based reduction approach cannot directly be applied here due to the frequency-dependency of the hydrodynamic matrices $\mathbf{M}_h(\omega)$ and $\mathbf{C}_h(\omega)$ in Eq. 1, which give rise to so-called motion-induced forces or radiation forces that are represented by convolution integrals in the time-domain. However, Eq. 1 is still linear, and it is possible to create a high-fidelity state-space model approximation. The details behind this type of state-space modeling, and in particular the handling of the motion-induced forces, is given in [8] and is excluded here for brevity. The result is a time-invariant reduced-order state-space model based on n_m selected modes, given in continuous form as:

$$\dot{\mathbf{x}}(t)=\mathbf{A}_c\mathbf{x}(t)+\mathbf{B}_c\mathbf{p}(t) \tag{4}$$

where $\mathbf{p}(t)\in\mathbb{R}^{n_m}$ contain the *modal* wave forces ($\mathbf{\Phi}^T\mathbf{L}_p\mathbf{p}_w(t)$) and $\mathbf{x}(t)\in\mathbb{R}^{n_s}$ is a state vector that takes into account the vibration modes as well as the motion-induced forces.

The output equation considering n_y acceleration or displacement measurements in the vector $\mathbf{y}(t)\in\mathbb{R}^{n_y}$ can be established as:

$$\mathbf{y}(t)=\mathbf{S}_a\ddot{\mathbf{u}}(t)+\mathbf{S}_d\mathbf{u}(t)=\mathbf{G}_c\mathbf{x}(t)+\mathbf{J}_c\mathbf{p}(t) \tag{5}$$

where $\mathbf{S}_a$ and $\mathbf{S}_d\in\mathbb{R}^{n_y\times n_{DOF}}$ are used to select the measured DOFs. The special definition of the state-space system matrices $\mathbf{A}_c\in\mathbb{R}^{n_s\times n_s}$, $\mathbf{B}_c\in\mathbb{R}^{n_s\times n_m}$, $\mathbf{G}_c\in\mathbb{R}^{n_y\times n_m}$ and $\mathbf{J}_c\in\mathbb{R}^{n_y\times n_m}$ are given in [8]. In our case

the state-space model of the Bergsøysund bridge is constructed using $\mathrm{n_m} = 18$ modes, with frequencies ω_j in the range $[0.6, 4]$ rad/s. The total number of system states is $\mathrm{n_s} = 180$.

We now discretize the state-space formulation by a time step Δt such that $t_k = k\Delta t$ ($k = 0, 1, \ldots, N_t - 1$), and consider the presence of stochastic noise:

$$\mathbf{x}_{k+1} = \mathbf{A}\mathbf{x}_k + \mathbf{B}\mathbf{p}_k + \mathbf{w}_k \tag{6}$$

$$\mathbf{y}_k = \mathbf{G}\mathbf{x}_k + \mathbf{J}\mathbf{p}_k + \mathbf{v}_k \tag{7}$$

where $\mathbf{x}_k = \mathbf{x}(t_k)$, $\mathbf{p}_k = \mathbf{p}(t_k)$ and $\mathbf{y}_k = \mathbf{y}(t_k)$. Assuming the force is constant between the sample instants ($t_k < t < t_{k+1}$), the discrete time system matrices can be shown to have the following definition:

$$\mathbf{A} = \exp\Big(\mathbf{A}_\mathrm{c}\Delta t\Big), \quad \mathbf{B} = (\mathbf{A} - \mathbf{I})\mathbf{A}_\mathrm{c}^{-1}\mathbf{B}_\mathrm{c}, \quad \mathbf{G} = \mathbf{G}_\mathrm{c}, \quad \mathbf{J} = \mathbf{J}_\mathrm{c} \tag{8}$$

The following covariance relations are used to describe the white-noise processes $\mathbf{w}_k \in \mathbb{R}^{\mathrm{n_s}}$ and $\mathbf{v}_k \in \mathbb{R}^{\mathrm{n_y}}$:

$$\mathbb{E}[\mathbf{w}_k\mathbf{w}_l^\mathrm{T}] = \mathbf{Q}\delta_{kl}, \quad \mathbb{E}[\mathbf{v}_k\mathbf{v}_l^\mathrm{T}] = \mathbf{R}\delta_{kl}, \quad \mathbb{E}[\mathbf{w}_k\mathbf{v}_l^\mathrm{T}] = \mathbf{S}\delta_{kl} \tag{9}$$

3 Methods for estimation of wave forces

3.1 Estimation by inverse identification algorithms

In this study we apply a joint input-state estimation algorithm [6, 7], which is a stochastic-deterministic method utilizing the system description in Eq. 6 and 7. The algorithm is a Kalman-type filter, where the input is unknown and thus jointly estimated with the system states. The filter equations are omitted here; the reader is referred to the cited references for an explanation of the algorithm.

It is chosen to identify modal forces ($\mathbf{p}(t)$) rather than the physical pontoon wave forces directly ($\mathbf{p}_\mathrm{w}(t)$). This necessary due to theoretical limitations of the number of forces that can be identified, which generally cannot exceed the number of acceleration outputs or the number of modes in the model [9]. Note that for algorithms with time-delayed inversion rather than instantaneous inversion, this criterion can for certain cases be given some slack [10]. In addition, it is an advantage to use modal forces when the additional unknown excitation from wind and traffic cannot be neglected, since any unmodelled sources of excitation conflicts with a system description where only localized inputs are considered. The modal forces covers by definition any kind of external loading to the system. We expect that the modal forces that are identified still should be dominated by the wave force content, since in comparison the wind and traffic excitation are much smaller.

3.2 Frequency-domain reconstruction using wave radar data

This sections shows idea behind the frequency-domain reconstruction of the wave forces, using a parametric model of the sea state together with a panel model of the pontoons.

We assume the sea surface elevation $\eta(x, y, t)$ is a zero-mean, homogeneous and stationary stochastic process. The wave field is described by the directional wave spectral density $S_{\eta\eta}(\omega, \theta) \in \mathbb{R}$, where θ represents the wave direction, which here is defined as the polar angle shown in Fig. 2. The one-dimensional wave spectrum $S_{\eta\eta}(\omega)$ can be obtained by integration over the directions:

$$S_{\eta\eta}(\omega) = \int_0^{2\pi} S_{\eta\eta}(\omega, \theta)\,\mathrm{d}\theta \tag{10}$$

The directional wave spectrum can be estimated from wave elevation measurements, for example by using the DIWASP Toolbox for MATLAB [11]. This toolbox implements the Extended Maximum Entropy Principle (EMEP) [12], a robust estimation method which utilizes the cross-spectral density of wave elevation measurements from a distributed array of wave radars.

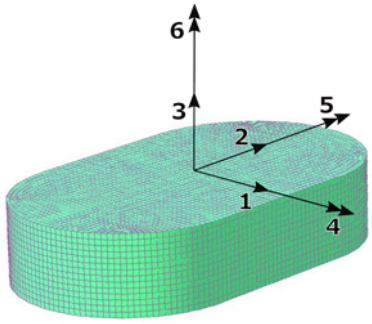

Figure 3: Panel model of the pontoon geometry. The numbers denotes the six local DOFs.

Provided that $S_{\eta\eta}(\omega,\theta)$ is known and equal at all the pontoon locations (homogenenous wave field), the cross-spectral density of the first-order wave forces on pontoon m can be calculated by the following integral:

$$S_{p_{\mathrm{w},i}^{(m)} p_{\mathrm{w},j}^{(m)}}(\omega) = \int_0^{2\pi} S_{\eta\eta}(\omega,\theta)\, Q_i^{(m)}(\omega,\theta-\alpha_m)\left(Q_j^{(m)}(\omega,\theta-\alpha_m)\right)^* \mathrm{d}\theta, \quad i,j=\{1\dots6\} \tag{11}$$

where the asterix denote the complex conjugate and $m \in \{1\dots7\}$ are indices for the seven pontoons. The subindexes i and j denote the six local DOFs, where $1-3$ are displacements and $4-6$ are rotations, see Fig. 3. $Q_i^{(m)}(\omega,\theta) \in \mathbb{C}$ is the directional transfer function relating wave elevation to the wave forces on pontoon number m, and depends on the incoming wave direction θ. α_m is the local rotation of the a pontoon with respect to the global xy-coordinate system ($\alpha_1 = 14°, \dots, \alpha_7 = -14°$). Finally, note that the formulation in Eq. 11 assumes the waves are fairly short-crested compared to the distance between two pontoons, which is reasonable since in this case the distance is ~ 105 m.

The transfer functions $Q_i^{(m)}(\omega,\theta)$ can be obtained by hydrodynamic codes. Here, we have created panel models of the pontoons in the software HydroD WADAM [13], with a geometry similar to the one shown in Fig. 3. The obtained transfer functions are shown in Fig. 4 and 5, using the middle pontoon ($m = 4$) as an example. The export resolution for the frequency and angle is set to 0.05 rad/s and $10°$, respectively.

To establish a global picture of wave loads, the power spectral density (PSD) matrix $\mathbf{S}_{\mathrm{p_w p_w}}(\omega) \in \mathbb{C}^{\mathrm{n_p}\times\mathrm{n_p}}$ containing all the wave forces ($\mathrm{n_p} = 7\times6 = 42$) is populated with the elements $S_{p_{\mathrm{w},i}^{(m)} p_{\mathrm{w},j}^{(m)}}(\omega)$ from Eq. 11. Since modal forces are identified with the inverse methods, $\mathbf{S}_{\mathrm{p_w p_w}}(\omega)$ can be transformed to the modal form $\mathbf{S}_{\mathrm{pp}}(\omega) \in \mathbb{C}^{\mathrm{n_m}\times\mathrm{n_m}}$ for a common basis of comparison:

$$\mathbf{S}_{\mathrm{pp}}(\omega) = \mathbf{\Phi}^{\mathrm{T}}\mathbf{L}_{\mathrm{p}}\mathbf{S}_{\mathrm{p_w p_w}}(\omega)(\mathbf{\Phi}^{\mathrm{T}}\mathbf{L}_{\mathrm{p}})^{\mathrm{T}} \tag{12}$$

4 Estimation of forces on the Bergsøysund bridge

4.1 Processing of the measurement data

A time series recorded 2017-10-29 12:39 with length 30 minutes is used in the full-scale identification. The acceleration and wave data is resampled to a sample rate of 10 Hz ($\Delta t = 0.1$ s), corresponding to $N_t = 1.8\cdot10^4$ time steps. In addition, the acceleration data is low-pass filtered to only include content below 4.5 rad/s. Above this limit, the contribution to the total response is negligible, and cannot be accounted for by the modal basis of the reduced-order state-space model. Sample time series from the wave radars and accelerometers are shown in Fig. 6 and 7, respectively. The peak wave frequency is 2.45 rad/s, which also leads to the highest dynamic response around this frequency.

For simplicity, only acceleration data and no displacement data is used in the inverse algorithms. In this case, this leads to a so-called marginally stable system inversion [9]. As will be shown, this mainly results

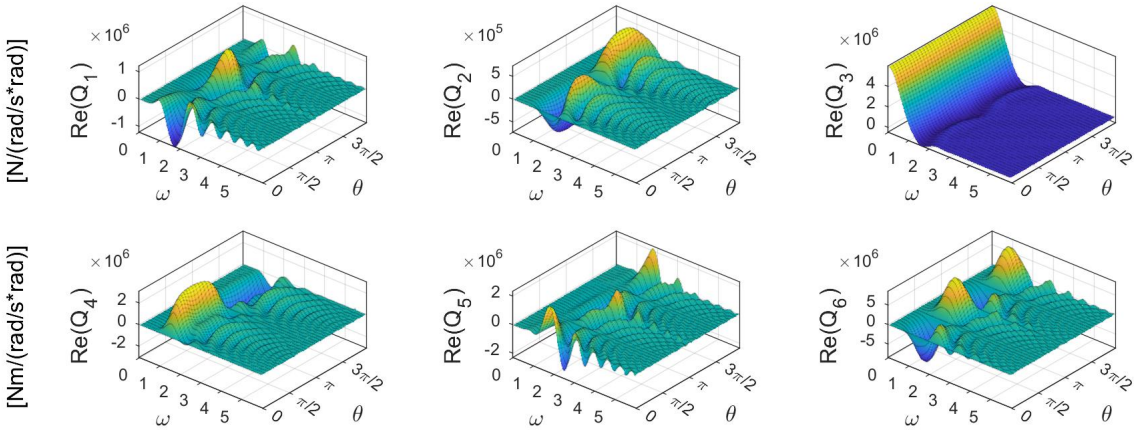

Figure 4: The real value of the transfer functions $Q_i(\omega, \theta)$ $(i = 1 \dots 6)$ for the middle pontoon.

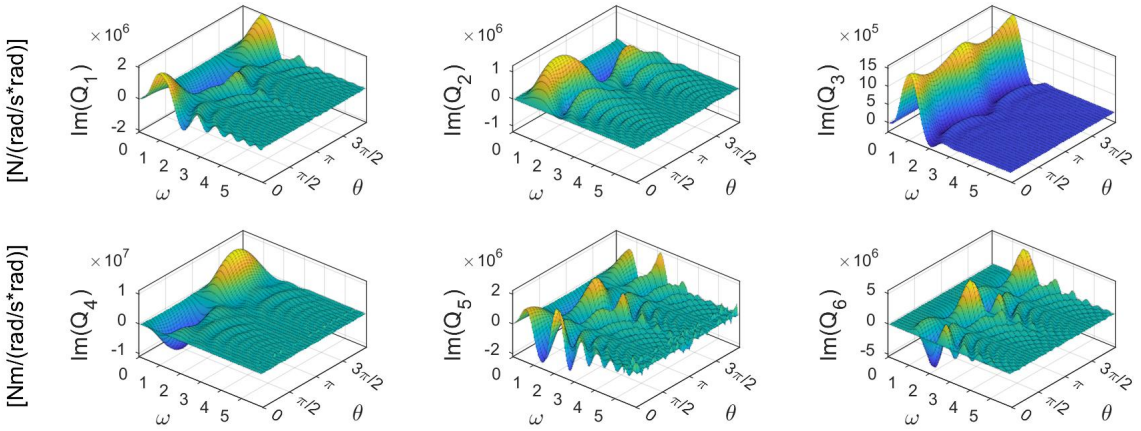

Figure 5: The imaginary value of the transfer functions $Q_i(\omega, \theta)$ $(i = 1 \dots 6)$ for the middle pontoon.

in spurious low-frequent content in the input estimates due to the lack of static-sensitive data, which is necessary to stabilize the filter solution.

The cross-spectral density between all the six wave radar measurements, which goes into the EMEP estimation, are calculated using a Welch-estimate with a section division of 512 samples and no overlap.

4.2 Force estimation results and discussion

The wave forces are now estimated using the methods presented in Section 3.1 and 3.2, respectively driven by acceleration data and wave elevation data.

The resulting estimate of the directional wave spectrum is illustrated in Fig. 8. The waves mainly approach from a skew angle of $65°$, coming from the fjord north of the bridge. Using the estimated directional wave spectrum, the modal waves forces are predicted using Eq. 11 and 12, as shown in Fig. 9. The figure also shows the PSD of the modal forces identified using the inverse algorithms. The covariance matrices $\mathbf{Q} = 10^{-2} \cdot \mathbf{I}$, $\mathbf{S} = \mathbf{0}$, $\mathbf{R} = 10^{-6} \cdot \mathbf{I}$ have been prescribed as the tuning variables for the filter.

Neglecting the frequency range $[0, 1]$ rad/s, the force estimates obtained from the two approaches are similar. Overall, this indicates that estimates of the forces are reasonable. A direct comparison of the forces obtained from the two methods should be interpreted with caution, however, since the methods are based on different assumptions. Both approaches are expected to have sources of uncertainties or assumptions that in reality are violated. The most important can be summarized as:

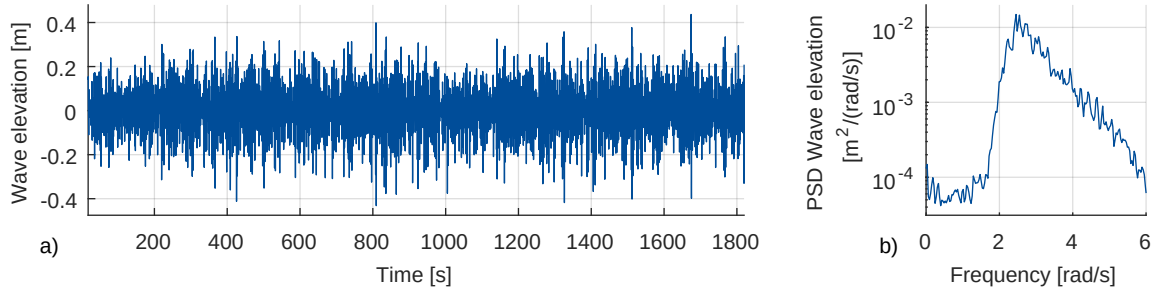

Figure 6: Sample wave elevation measurement from one of the wave radars.

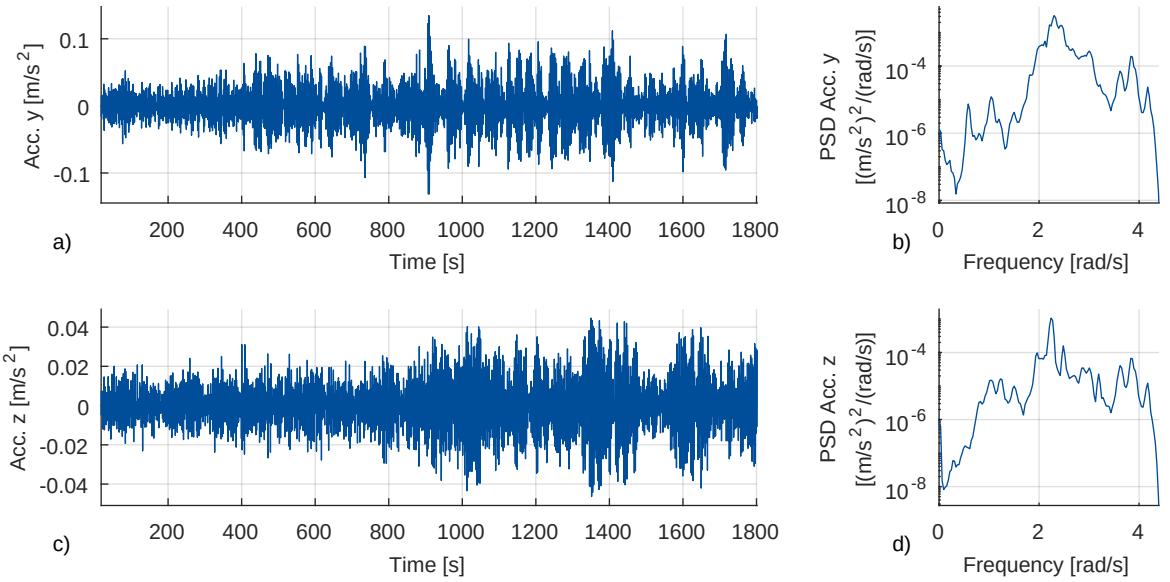

Figure 7: Sample acceleration measurements from pontoon number 3 in the horizontal (y) and vertical (z) direction. The data is low-pass filtered below 4.5 rad/s.

- Errors on the state-space model, coming from model errors in the structural finite element model or the model for the fluid-structure interaction.
- Sensor uncertainty in the accelerometers and wave radars, in particular for the low-frequent range below 1 rad/s.
- EMEP estimation errors of the directional wave field, leading to for example waves approaching from unlikely directions such as 180° in Fig. 8 a.
- Inhomogeneities of the global wave field in the strait cannot be detected when the wave radars are clustered closely together (cf. Fig. 2 a).
- Multibody pontoon interaction through the fluid is not considered here. This influences the transfer functions $Q_i^{(m)}(\omega, \theta)$, as well as $\mathbf{M}_\mathrm{h}(\omega)$ and $\mathbf{C}_\mathrm{h}(\omega)$ and so also the state-space model.
- Second-order sum and difference wave forces are not considered in the wave force reconstruction.
- Presence of additional excitation (wind or traffic) will show up in the identified forces, although their magnitude is small when compared to the wave loads.

Further work should consider more recordings from the measurement database with various ambient wave conditions, such as SWH, wave direction and peak frequency.

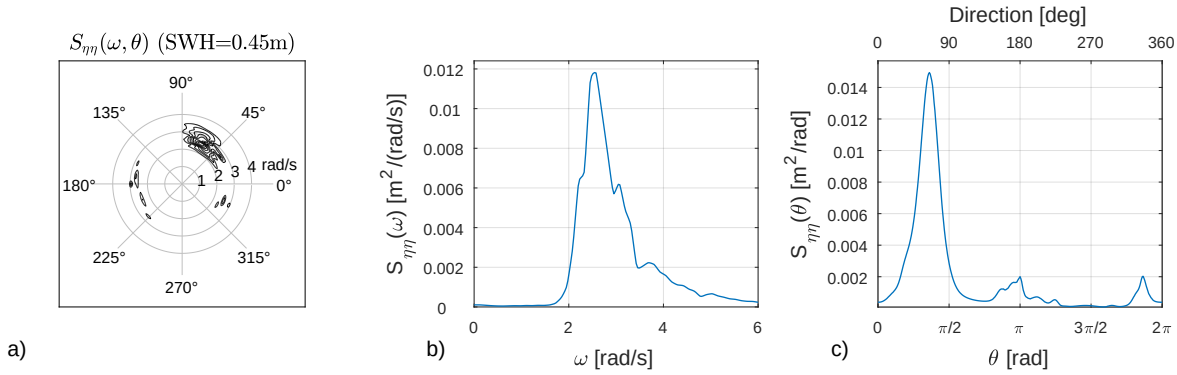

Figure 8: a) Estimated directional wave spectrum using EMEP in the DIWASP Toolbox; b) marginal wave spectrum for frequency only; c) marginal wave spectrum for direction only.

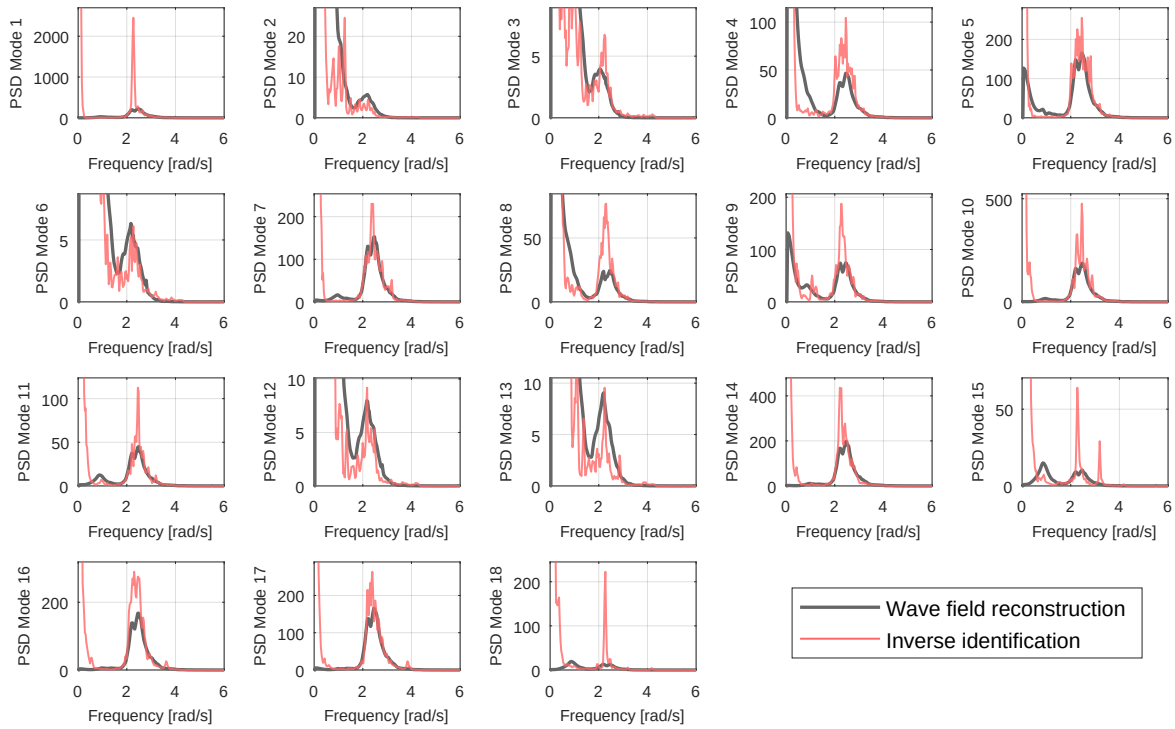

Figure 9: Auto PSD of the estimated modal forces for all the 18 modes. Both the force estimate from the wave field reconstruction and the input estimate from the inverse identification is shown.

5 Conclusion

This paper has presented has presented a case-study of the full-scale identification of wave forces on a floating bridge. Two different approaches was used: 1): force identification by a joint input-state estimation algorithm using measured acceleration data; 2): frequency-domain reconstruction of the forces using measured wave elevation data. The force estimates obtained from the two methods appear to have a reasonable agreement when compared in the frequency-domain. The discrepancies that occur can be explained by the different simplifications, modelling uncertainties and assumptions behind the two methods. The study shows that different approaches for obtaining the ambient forces have advantages and disadvantages, so that the methods can complement each other in the total assessment of the forces.

Acknowledgements

We gratefully acknowledge the financial support from the Norwegian Public Roads Administration.

References

[1] Y. Xu, O. Øiseth, T. Moan, *Time domain simulations of wind-and wave-induced load effects on a three-span suspension bridge with two floating pylons*, Marine Structures, Vol. 58, (2018), pp. 434-452.

[2] Z. Cheng, Z. Gao, T. Moan, *Wave load effect analysis of a floating bridge in a fjord considering inhomogeneous wave conditions*, Engineering Structures, Vol. 163, (2018), pp. 197-214.

[3] K. Kvåle, O. Øiseth, *Structural monitoring of an end-supported pontoon bridge*, Marine Structures, Vol. 52, (2017), pp. 188-207.

[4] K. Kvåle, O. Øiseth, A. Rønnquist, *Operational modal analysis of an end-supported pontoon bridge*, Engineering Structures, Vol. 148, (2017), pp. 410-423.

[5] Ø.W. Petersen, O. Øiseth, T.S. Nord, E. Lourens, *Estimation of the full-field dynamic response of a floating bridge using Kalman-type filtering algorithms*, Mechanical Systems and Signal Processing, Vol. 107, (2018), pp. 12-28.

[6] E. Lourens, C. Papadimitriou, S. Gillijns, E. Reynders, G. De Roeck, G. Lombaert, *Joint input-response estimation for structural systems based on reduced-order models and vibration data from a limited number of sensors*, Mechanical Systems and Signal Processing, Vol. 29, (2012), pp. 310-327.

[7] K. Maes, A.W. Smyth, G. De Roeck, G. Lombaert, *Joint input-state estimation in structural dynamics*, Mechanical Systems and Signal Processing, Vol. 70-71, (2012), pp. 445-466.

[8] Ø.W. Petersen, O. Øiseth, *Efficient time-domain modeling of floating structures with fluid-structure interaction by reduced order state-space approximations*, *Submitted to the 28th Conference on Noise and Vibration Engineering, Leuven, Belgium, 2018*.

[9] K. Maes, E. Lourens, K. Van Nimmen, E. Reynders, G. De Roeck, G. Lombaert, *Design of sensor networks for instantaneous inversion of modally reduced order models in structural dynamics*, Mechanical Systems and Signal Processing, Vol. 52, (2014), pp. 628-644.

[10] K. Maes, S. Gillijns, G. Lombaert, *A smoothing algorithm for joint input-state estimation in structural dynamics*, Mechanical Systems and Signal Processing, Vol. 98, (2018), pp. 292-309.

[11] D. Johnson, *DIWASP, a directional wave spectra toolbox for MATLAB: User manual*, Research Report WP-1601-DJ (V1.1), Centre for Water Research, University of Western Australia, (2012).

[12] N. Hashimoto, T. Nagai, T. Asai, *Extension of the maximum entropy principle method for directional wave spectrum estimation*, in B. Edge, editor, *Proceedings of 24th Conference on Coastal Engineering, 1994, Kobe, Japan*, Kobe (1994), pp. 232-246.

[13] DNV Software, *HydroD WADAM 9.1 User Manual*, Høvik, Norway, (2014).